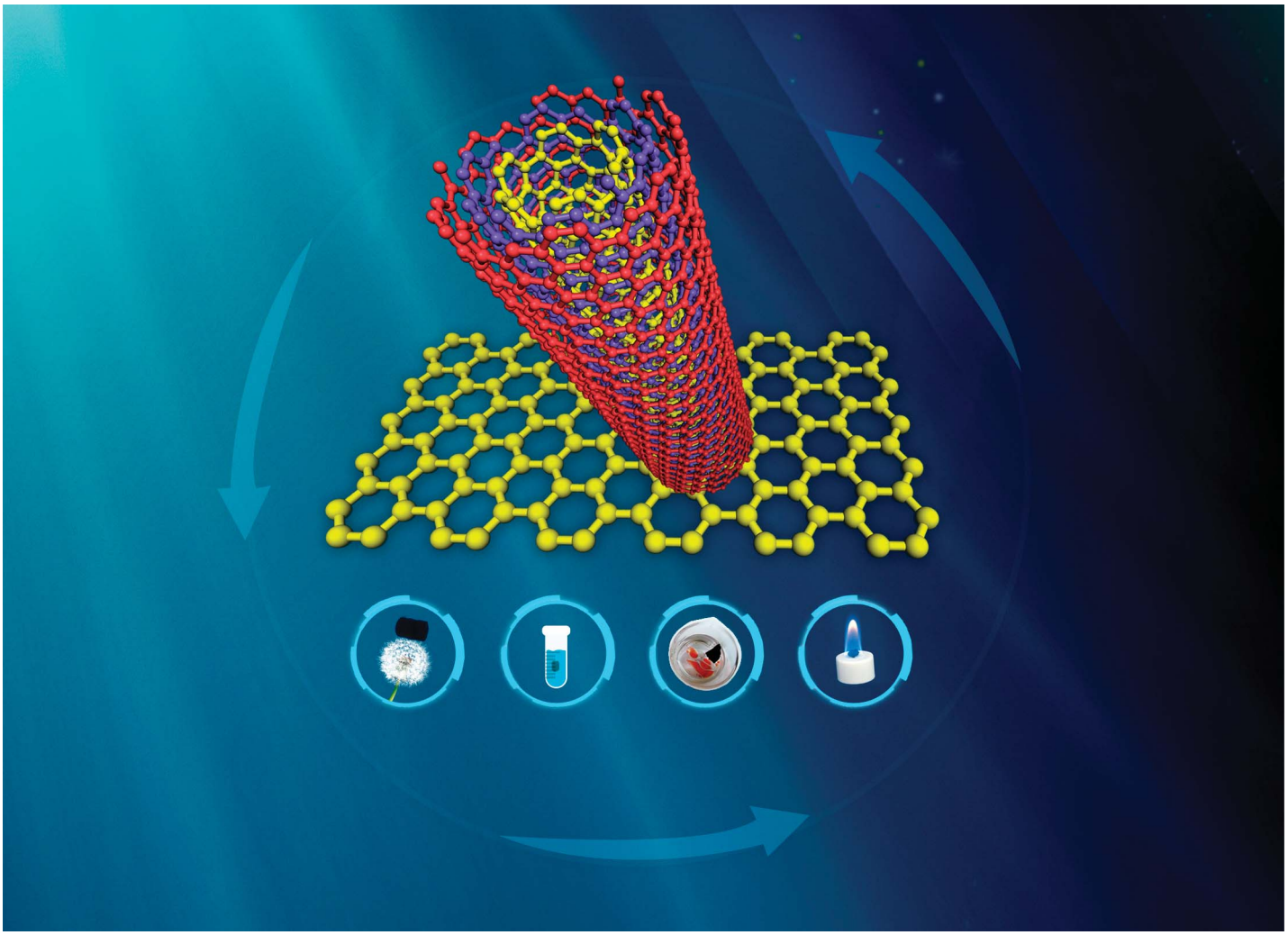

Showcasing research on the macroscopic self-assembly of low-dimensional carbon materials and their functionalities by Prof. Tao Yi at Department of Chemistry, Fudan University and Prof. Jin Zhang at College of Chemistry and Molecular Engineering, Peking University, China.

Title: Density controlled oil uptake and beyond: from carbon nanotubes to graphene nanoribbon aerogels

The relationship of oil adsorption capacity and carbon-based aerogel parameters has been fabricated, and a brand-new concept of aerogel-based densitometers is demonstrated, paving the way for designing superior sorbents and expanding the application territory of aerogels.

As featured in:

See Jin Zhang, Tao Yi *et al.*, *J. Mater. Chem. A*, 2015, **3**, 20547.

ROYAL SOCIETY OF CHEMISTRY

www.rsc.org/MaterialsA

Registered charity number: 207890

Journal of Materials Chemistry A

PAPER

View Article Online
View Journal | View Issue

Cite this: J. Mater. Chem. A, 2015, 3, 20547

Density controlled oil uptake and beyond: from carbon nanotubes to graphene nanoribbon aerogels†

Liang Chen,‡[a] Ran Du,‡[b] Jin Zhang*[b] and Tao Yi*[a]

Large-scale manipulation of the density (from 2.5 to 1327 mg cm^{-3}) and wettability of carbon-based aerogels has been realized by delicately modulating the gelation, drying and post-treatment processes. An unexpected "Janus face" effect of pyrrole was revealed in the fabrication process. Pyrrole acts as a "spacer" at relatively low concentrations (<*ca.* 5 vol%), resulting in a decrease of the aerogel density; however, "linker" behaviour appears at higher concentrations (>*ca.* 5 vol%), leading to an increase of the aerogel density. By using systematic studies, the oil adsorption capacity of aerogels has been correlated with the aerogel density and surface wettability, which can guide the production of highly efficient sorbents. For example, a polydimethylsiloxane modified graphene nanoribbons aerogel with a density of 2.5 mg cm^{-3} was prepared and showed a remarkable adsorption capacity of up to 302 times for phenixin and 121 times for *n*-hexane its own weight, much higher than that of most carbonaceous sorbents previously reported. Furthermore, a proof-of-concept aerogel-based floating-type densitometer has also been proposed to expand the potential applications of aerogels.

Received 16th June 2015
Accepted 17th July 2015

DOI: 10.1039/c5ta04370k

www.rsc.org/MaterialsA

Introduction

With the rapid development of modern industry, environmental and ecological problems arising from organic spills (*e.g.*, petroleum products or toxic organic solvents) in water have become increasingly serious. Water pollution not only increases the risks to the drinking water supply of growing populations, but it also poses fatal threats to living species.[1,2] To address this problem, adsorbents based on mesoporous silica, resin, expanded graphite, activated carbon, and so on have been developed to remove oil spills from water.[3–7] However, low oil-sorption capacity and poor water/oil selectivity limit their wide use. Meanwhile, microporous polymers have also been considered because of their ultrahigh specific surface area and hydrophobicity.[8–12] However, the dominant microporosity (ion-inaccessible) and high production cost cast a shadow on their practical applications. In recent years, carbonaceous materials have attracted great attention in water remediation because of their low weight, high stabilities (*e.g.*, thermal, chemical-stability) and eco-friendliness. However, the small size of the unassembled carbon-based powder materials is difficult to recycle after use, which can cause serious secondary pollution and raise the use-cost.[2]

In the past few years, carbon-based three-dimensional (3D) architectures have been widely developed and studied as a new generation of efficient oil adsorbents.[13–22] Compared with traditional sorbents, the macroscopically monolithic structures of those 3D carbon-based materials facilitate easy collection and recycling, eliminating secondary pollution and decreasing the use-cost. Additionally, interconnected macro- and meso-porous structures obtained from the assembly process create high-speed mass transfer channels for rapid sorption. From the perspective of adsorption capacity (expressed by the weight gain compared with the original weight of the sorbents), the performance of sorbents has been improved from the initial parameters of tens of times (*e.g.*, spongy graphene[14]) to hundreds of times (*e.g.*, carbon nanotube (CNT) sponges,[16] carbon fibre aerogels,[15] nitrogen-doped graphene frameworks[18]), recently reaching 1010 times, as recorded by unique graphene sponges.[19]

With such great potential for oil adsorption, determining the structure–performance relationship of carbon-based aerogels is important to guide materials design and further promote application performance. Unfortunately, although the synthetic methods and sorption performance have been widely reported,[15–17,23–25] an in-depth understanding of the relationship

[a]Department of Chemistry, Collaborative Innovation Center of Chemistry for Energy Materials, Fudan University, Shanghai 200433, P. R. China. E-mail: yitao@fudan.edu.cn

[b]Center for Nanochemistry, Beijing National Laboratory for Molecular Sciences, Key Laboratory for the Physics and Chemistry of Nanodevices, State Key Laboratory for Structural Chemistry of Unstable and Stable Species, College of Chemistry and Molecular Engineering, Peking University, Beijing 100871, P. R. China. E-mail: jinzhang@pku.edu.cn

† Electronic supplementary information (ESI) available: Preparation methods of aerogels, SEM images, TEM images, XRD spectra, EDX mapping and other characterization. See DOI: 10.1039/c5ta04370k

‡ L. Chen and R. Du contributed equally to this work.

between the adsorption capacity and physical parameters of aerogels (especially density and wettability) is still unexplored. One possible reason for this lack of understanding lies in the absence of effective methods to modulate these physical parameters across a wide range. Conversely, carbon-based aerogels have many attractive features (*e.g.*, very low density, high porosity, high stability, and free-standing form), so there is great potential to expand their applications.

Previously, nitrogen-doped aerogels were fabricated based on graphene nanoribbons (GNRs), CNTs bridged with GNRs (CNTs@GNRs), and CNTs for the oxygen reduction reaction (ORR) by a promoter-assisted hydrothermal reaction coupled with pyrolysis in our lab.[26–28] Based on a thorough understanding of gelation mechanisms and systematic studies, this study presents a large-scale manipulation of the density (from 2.5 to 1327 mg cm^{-3}) and wettability of carbon-based aerogels by modulating the gelation, drying and post-treatment processes, thus fabricating the structure–performance relationship. Furthermore, as an example of expanding the applicability of carbon-based aerogels, a new aerogel-based floating-type densitometer is demonstrated.

Results and discussion

The preparation method of carbon-based hydrogels is schematically illustrated in Fig. 1, where the mixture of pyrrole and the carbon precursor aqueous solution (*e.g.*, oxidized MWNTs (ox-MWNTs), partially unzipped MWNTs (CNTs@GONRs) and graphene oxide nanoribbons (GONRs)) was subjected to a hydrothermal reaction (HTR) to generate uniform hydrogels. Then, the as-prepared hydrogels were directly dehydrated *via* a freeze-drying process to maintain the 3D monolithic architecture, generating carbon-based aerogels. Some samples received further pyrolysis processing. The XRD patterns of the precursors and the corresponding TEM images of the aerogels are also provided in the ESI (ESI, Fig. S1 and S2†).

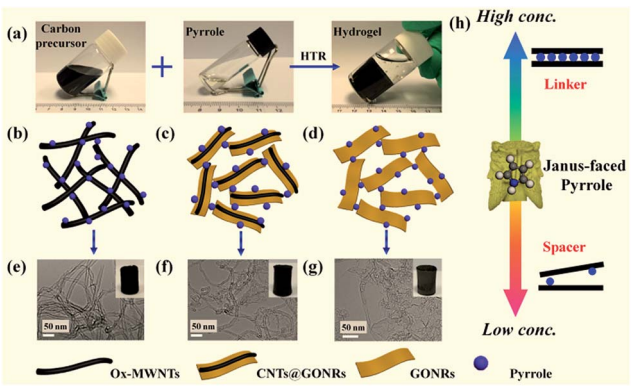

Fig. 1 (a) Illustration of the preparation of carbon-based aerogels; (b–d) schematic structures of MWNTs, CNTs@GNRs, and GNR aerogels; (e–g) the corresponding TEM images and digital photos (inset) of (b–d), respectively; (h) "Janus face" of pyrrole molecules as either linkers or spacers.

Gelation mechanism

Gelation was achieved through a combination of interactions between carbon precursors (π–π interactions) and carbon precursors and pyrrole (hydrogen bonds of N–H···O, π–π interactions).[18,28] The π–π interactions between oxidized carbon precursors are enhanced by the hydrothermal reduction effect, so GONRs eventually turn into gels because of the efficient π–π interactions between the planar graphene flakes.[26,29,30] However, for CNTs@GONRs and ox-MWNTs, the π–π interactions between adjacent carbon precursors are less effective (especially at a low concentration) for self-assembly because of their tubular geometries, thus causing easy dislocation between building blocks and requiring an extra crosslinking force.[13,26–28] Therefore, pyrrole was utilized to provide an additional support to hold the 3D networks through synergistic interactions with carbon precursors. In other words, during the gelation process, pyrrole is the main physical "crosslinker" for ox-MWNTs and CNTs@GONRs (because of less-effective π–π interactions between carbon precursors), but a physical "co-crosslinker" for GONRs (GONRs themselves can also serve as crosslinkers because of effective inter-sheet π–π interactions).

Unexpectedly, when the pyrrole concentration was varied, more complicated roles of pyrrole appeared. Pyrrole showed a "Janus face" during the assembly process (Fig. 1h), which acted as a "spacer" at lower concentrations (c_{py}) but exhibited "linker-like" behaviour at higher concentrations, especially for the case of GONRs.

Pyrrole possesses both a hydrogen bond donor and an aromatic ring that is capable of bonding oxidized carbon precursors *via* hydrogen bonding or π–π stacking. At a lower c_{py} (<*ca.* 5 vol%), the total bonding force is weak because of the small amount of bonds between pyrrole and the carbon precursors. Therefore, on this occasion, pyrrole could be regarded as an inert spacer that can shield the π–π interaction between carbon precursors and effectively prevent the self-stacking of carbon precursors,[30] thus expanding the gel volume of the resultant GNR gel (Fig. S3†). In this case, the main crosslinking force originated from the π–π interactions between π-conjugated backbones. Unlike GONRs, ox-MWNTs and CNTs@GONRs cannot gel in the low c_{py} region due to less efficient π–π stacking between adjacent carbon precursors, as previously described. However, at a higher c_{py} (>*ca.* 5 vol%), the crosslinking force is greatly enhanced and the linker effect of pyrrole becomes dominant. As a result, for all carbon precursors, the obtained gels showed obvious volume shrinkage with increasing pyrrole concentration (Fig. S3a–c†). Therefore, the apparent density of the final aerogel increases with increasing crosslink density. The above analysis was also supported by SEM images (Fig. S3d–l†) in which the aerogel morphology became apparently more compact with the increasing pyrrole concentration in the higher c_{py} region, while the morphology became extended with the increasing pyrrole concentration in the lower c_{py} region. With a deep understanding of the gelation mechanism, it is possible to manipulate the density of the corresponding aerogels (ρ) by controlling the crosslinking force during the gelation step, as discussed below.

Density control of aerogels

Density is one of the most important parameters for aerogel applications. Although some research showed the tunability of aerogel densities,[17,24,31,32] in-depth systematic investigations of the internal mechanism are absent; large-scale modulation has not been achieved. Therefore, it is desirable to conduct systematic studies on density control across a wide range.

Type of carbon precursors

Compared with the original CNTs, GNRs derived from CNTs exhibit more 2D features because of their smaller in-plane aspect ratio (theoretically $1/\pi$ of CNTs), thus they possess more efficient π–π stacking, with a larger plane overlap. Therefore, GONRs can form gels at a lower c_{py} (<5 vol%). In contrast, CNTs@GONRs and ox-MWNTs can only form gels at a higher c_{py} (>5 vol%), where the "linker effects" of pyrrole are in the lead. As shown in Fig. 2a, under the optimized conditions, GNR aerogels showed a much lower density (~2.5 mg cm^{-3}) compared with CNTs@GNRs (~9.7 mg cm^{-3}) and MWNT aerogels (~13.4 mg cm^{-3}). Therefore, the aerogel density can be controlled by designing carbon precursors with different dimensionalities to acquire optimal interactions.

Pyrrole concentration

As described above, pyrrole exhibited a contrary behaviour at different concentration regions. Fig. S3a–c† illustrate that when the pyrrole concentration is above 5 vol%, the density of all three carbon precursor-based aerogels increased with increasing c_{py}, indicating the "linker effects" of pyrrole. However, for GNRs, the hydrogel underwent a considerable volume expansion (together with a density decrease of the corresponding aerogel), with pyrrole increasing from 0 vol% to 5 vol% (Fig. S3c†), suggesting "spacer effects" of pyrrole at a lower c_{py}. It should be noted that when the concentration of carbon precursors is 5 mg mL^{-1}, the minimum gelation concentration of pyrrole for ox-MWNTs and CNTs@GONRs is determined as approximately 8 vol% and 5 vol%, respectively. By controlling and utilizing the role of pyrrole at different concentration regions, a large range (~2 orders of the magnitude) modulation of the aerogel density was achieved (Fig. 2b). This wide range density control paved the way for acquiring a large-scale structure–performance picture of aerogels used for oil adsorption.

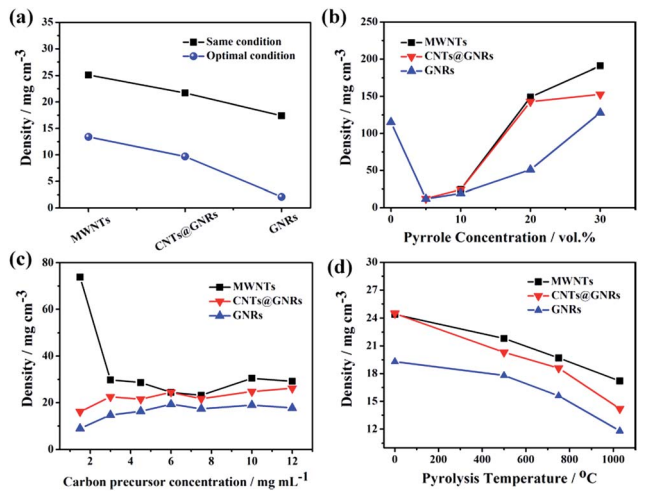

Fig. 2 Illustration of the density control of carbon-based aerogels. The density evolution with (a) carbon precursors (for the same condition, the initial carbon precursor concentration c_0 = 7.5 mg mL^{-1}, and pyrrole concentration c_{py} = 10 vol%; for the optimal conditions, GNRs, c_0 = 1.0 mg mL^{-1}, c_{py} = 5 vol%, pyrolysis at 1030 °C; CNTs@GNRs, c_0 = 5.0 mg mL^{-1}, c_{py} = 5 vol%, pyrolysis at 1030 °C; MWNTs, c_0 = 7.5 mg mL^{-1}, c_{py} = 10 vol%, pyrolysis at 1030 °C), (b) pyrrole concentration (c_0 was fixed at 5 mg mL^{-1}), (c) initial carbon precursor concentration (c_{py} was fixed at 10 vol%) and (d) pyrolysis temperature (c_0 and c_{py} were fixed at 7.5 mg mL^{-1} and 10 vol%, respectively).

Concentration of carbon precursors

The initial carbon precursor concentration also played a significant role in determining the density of the resultant aerogels (Fig. 2c and S4†). For a given pyrrole concentration, the density of GNRs and CNTs@GNR aerogels slightly increased with the increase of precursor concentration. This may occur because the quasi-2D geometry of GNRs generated strong π–π interactions even at low concentrations, identical to graphene aerogels reported elsewhere.[18,33,34] Therefore, interactions between carbon precursors (*i.e.*, π–π interactions) overwhelmed the "linker effects" introduced by pyrrole, leading to a continuously increased density with an increasing carbon precursor concentration. However, the density of MWNT aerogels experienced a minimal value (7.5 mg mL^{-1}) in the density–concentration curve of MWNT aerogels due to the coexistence of the reduced "linker effects" and enhanced π–π interactions with the increasing MWNT concentration. The increased concentration of MWNTs gives rise to a decreased pyrrole/MWNT ratio, which reduced the "linker effects" of pyrrole and thus decreased the density of the aerogel. The increased MWNT concentration enhanced the π–π interactions between the adjacent MWNTs, leading to the enhanced crosslinking force and increased aerogel density.

Drying method

The transition process from hydrogels to aerogels can also be modulated to tailor the density of aerogels. Generally, freeze-drying and supercritical CO_2 drying are frequently used to create low-density aerogels ranging from several to several tens of milligrams per cubic centimetre by reducing the surface tension (σ) variation around the gel networks before and after drying.[10,24] In contrast, conventional heat-drying was generally employed to achieve more compact aerogels (with high density). In this way, the solvents inside the gels were evaporated to gas by directly crossing the gas–liquid phase line, which induced a considerable aggregation of the gel networks and remarkably increased the density.[29] The aggregation degree was directly correlated with the surface tension of the solvent in wet gels, so the aerogel density can be modulated stepwise by exchanging the water in hydrogels with solvents with different surface tensions. As shown in Fig. S5,† the density of aerogels was

linearly increased, and the morphology became more compact with the increasing surface tension of the gelling solvents, from *n*-pentane (ρ_{MWNTs}: 100.0 mg cm^{-3}, ρ_{GNRs}: 360.32 mg cm^{-3}, σ: 16 mN m^{-1}), *n*-hexane (ρ_{MWNTs}: 115.6 mg cm^{-3}, ρ_{GNRs}: 432.58 mg cm^{-3}, σ: 18.4 mN m^{-1}) and toluene (ρ_{MWNTs}: 163.0 mg cm^{-3}, ρ_{GNRs}: 645.2 mg cm^{-3}, σ: 28.5 mN m^{-1}) to water (ρ_{MWNTs}: 350.7 mg cm^{-3}, ρ_{GNRs}: 1327.1 mg cm^{-3}, σ: 72.8 mN m^{-1}). This phenomenon also suggested that the density of GNR aerogels was much more sensitive to the drying medium than that of MWNT aerogels, which may be attributed to more efficient π–π stacking between quasi-2D GNRs compared to MWNTs. Consequently, it is easier to re-stack the aerogels to form graphite-like structures during the heat-drying process.

Pyrolysis

In addition, to modulate the crosslinking force during the gelation period and alter the drying process, the aerogel density can also be controlled by a post-treatment. It was known that pyrolysis can effectively reduce graphene oxide by deoxygenation under high temperature, resulting in significant mass loss.[35] For aerogels derived from oxidized carbon precursors in this case (*i.e.*, ox-MWNTs, CNTs@GONRs and GONRs), a similar process occurred under post-pyrolysis. Although aerogels experienced some volume shrinkage during pyrolysis, the net result led to a gradual density decrease with increasing pyrolysis temperature, as shown in Fig. 2d. In this way, a 25–45% density decrease could be achieved.

Oil uptake

Oil uptake is one of the most relevant applications for aerogels.[2] Its performance should be related to the aerogel densities, but without strict confirmation. Additionally, the wettability of solution-derived aerogels remains a large problem that affects their efficiency in the treatment of practical oil/water mixture systems.

Density-controlled oil uptake

By modulating the aerogel densities using the above methods, the correlation between the density and the oil uptake capacity was established. As shown in Fig. 3a, the aerogel density was plotted *versus* the adsorption capacity of bromobenzene (expressed by the weight gain of aerogels after adsorption) in a wide range. The curve indicated that the adsorption capacity rapidly increased with decreasing aerogel density, following a power function (Fig. S6†), from ~740 wt% for 191 mg cm^{-3}, to ~27 630 wt% for 2.5 mg cm^{-3}. It was known that the porosity (η) of aerogels was linearly correlated with the apparent aerogel density (ρ_{app}) (see ESI†).[29] Assuming that the bulk density of MWNTs (~2.1 g cm^{-3}) was approximately equal to that of GNRs (~2.2 g cm^{-3}),[36,37] the oil uptake capacity was also correlated with aerogel porosity following a similar power function (Fig. S7a†). This means that for a given organic solvent (oil), an aerogel with a larger porosity (*i.e.*, larger pore volume) can accommodate more solvents.

Notably, the pore volume (V_a) described in this study was entirely different from the value given by the nitrogen adsorption measurement (typically less than 4 cm^3 g^{-1}) where only mesopores were considered.[29] For oil uptake, the pore volume of all pore sizes, especially macropores, should be included. The pore volume could be simply calibrated as described in the ESI,† where a value of ~199.5 cm^{-3} g^{-1} was obtained assuming an aerogel with a density of 5 mg cm^{-3}. Similarly, it was also meaningless to correlate the oil uptake capacity with a specific surface area derived from the nitrogen adsorption measurement (typically reflecting the information of mesopores and micropores depending on the selected pressure range for calculation). As shown in Fig. S7b,† the oil uptake capacity showed an ambiguous relationship *versus* either the BET surface area or the pore volume derived from the nitrogen adsorption measurement.

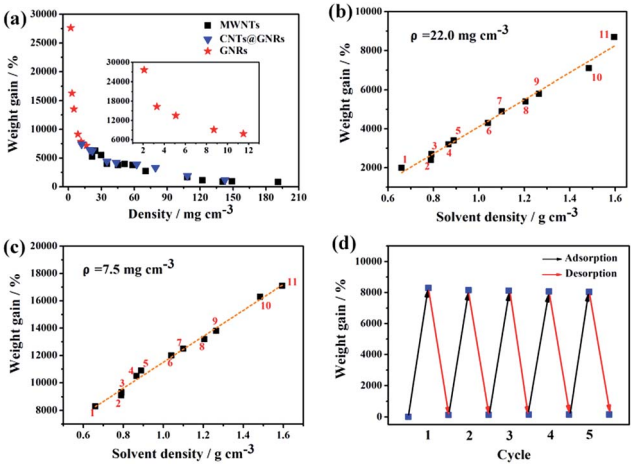

Fig. 3 Oil uptake performance of aerogels. (a) Density-dependent oil uptake (using bromobenzene as an example) of carbon-based aerogels with various densities; (b–c) adsorption capacity of GNR aerogels (density of 22.0 and 7.5 mg cm^{-3}) towards a wide range of organic solvents with different densities. The numbers 1–11 represent *n*-hexane, ethanol, methanol, toluene, THF, benzyl alcohol, DMSO, nitrobenzene, glycerol, chloroform and phenoxin, respectively; (d) recyclability of a piece of a GNR aerogel by alternate absorption and release of *n*-hexane under heat treatment (85 °C) for five cycles.

To further investigate the oil uptake mechanism, the adsorption capacity of the aerogel (using the GNR aerogel as an example) towards a wide range of organic solvents with different densities was measured (Fig. 3b–c and S8†). The weight gain of the aerogel was linearly correlated with the solvent density, meaning that a certain volume of the aerogel was occupied nearly irrespective of the solvent properties (*e.g.*, density, dipole moment). This also lays the foundation for using the aerogel for a new type of densitometer that will be described later.

Combining the above analyses, it can be concluded that a lower density of carbon-based aerogels would significantly increase the oil uptake capacity and that the volume of the adsorbed solvents was nearly independent of their properties. For example, the aerogel with a density of 2.5 mg cm^{-3} exhibits an excellent adsorption performance, with the adsorption capacity reaching as high as 120–302 times its own weight, which is much higher than that of most carbonaceous sorbents previously reported (see Fig. S8 and Table S1†). Therefore, the

design of carbon-based aerogels with ultralow density was preferred for realizing superior oil uptake performance.

Furthermore, as a type of promising adsorption material, the recyclability of the aerogel and the recoverability of the organic solvents are key standards for organic pollutant clean up applications. With this in mind, the recycling potential of the resulting aerogel was investigated through "evaporation" or combustion in the air (Fig. S9†) using *n*-hexane as an example. In general, after adsorption, the sample was heated to the boiling point to release the absorbed liquid. Then, the vapour of the liquid was collected for recycling. As shown in Fig. 3d, the aerogels still retained their ultrahigh absorption capability after six absorption–distillation cycles, suggesting their great potential as a new super-adsorption material with high-efficiency and recyclability.

Oil uptake in the oil/water system

The solution for practical environmental problems continually requires addressing the oil/water mixture system, where high oil/water selectivity is greatly desired. Surprisingly, although many reported carbon-based aerogels showed high adsorption capacity, not all showed adequate hydrophobicity. As shown in Fig. S10a–d,† the contact angles of aerogels prepared by the present method are zero, irrespective of post-pyrolysis. The same case was also found for the graphene aerogel derived from the graphene oxide solution with or without the introduction of pyrrole (Fig. S10c–f†). In some cases, however, although the aerogel seemed to be initially hydrophobic, the water gradually penetrated into the gel networks over a few minutes and finally exhibited a zero contact angle. Therefore, when these aerogels were added into an oil/water mixture, a substantial adsorption capacity loss appeared because of the competitive water adsorption. In this regard, a low-surface-energy coating was required to strengthen the aerogel hydrophobicity.[38,39]

A super-hydrophobic surface could be facilely created by a vapour deposition method assisted with polydimethylsiloxane (PDMS).[40,41] Thanks to the open pores of the aerogel, by simply co-heating the aerogel with PDMS, the evaporated PDMS oligomers easily penetrated into the aerogel and formed a conformal layer on surfaces throughout the entire aerogel (Fig. S11†). In this way, highly hydrophobic aerogels with a contact angle of ~140° could be created by a treatment for approximately 10 minutes with fresh PDMS without large morphology change (Fig. 4a–d).

Energy dispersive X-ray spectroscopy (EDX) mapping showed a uniform distribution of silica elements (Fig. S12†), suggesting a homogeneous coating of PDMS short chains on the aerogel networks. PDMS loading could be facilely tuned by altering the

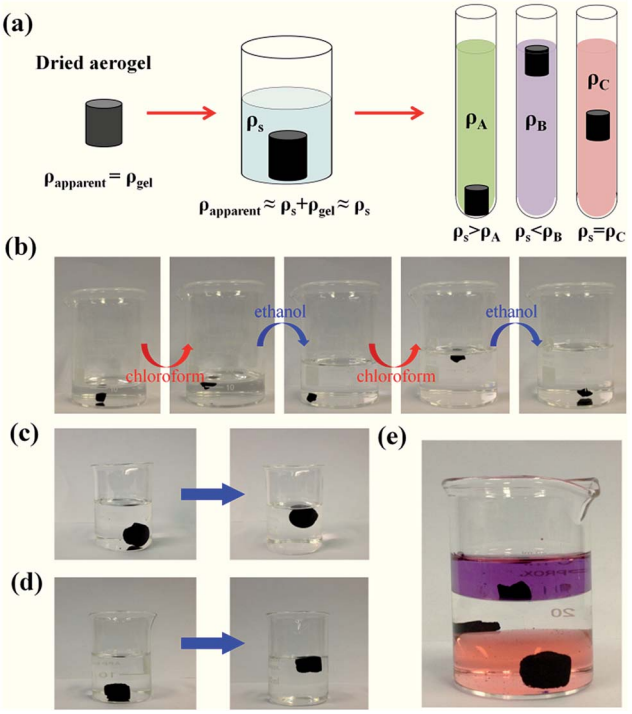

Fig. 5 The use of aerogels as floating-type densitometers. (a) Mechanism of aerogel-based floating-type densitometers. (b) Photograph showing that the toluene (relative density $\rho = 0.87$) saturated aerogel floats up and down reversibly upon alternatively tuning the solution density by adding chloroform ($\rho = 1.489$) and ethanol ($\rho = 0.79$), indicating that the aerogel could show different floating states related to the solution density. (c) The aerogel saturated in DMF ($\rho = 0.9445$) could float up in pyridine ($\rho = 0.9827$); (d) the aerogel saturated in chloroform ($\rho = 1.489$) could float up in bromobenzene ($\rho = 1.495$), indicating that the aerogel could monitor a density difference of less than 0.006 g mL^{-1}. (e) The liquid from the top to the bottom was *n*-hexane ($\rho = 0.66$, dyed with Sudan Black B), water and chloroform (dyed with Sudan III). The aerogel from the top to bottom was saturated by *n*-hexane, water and phenoxin.

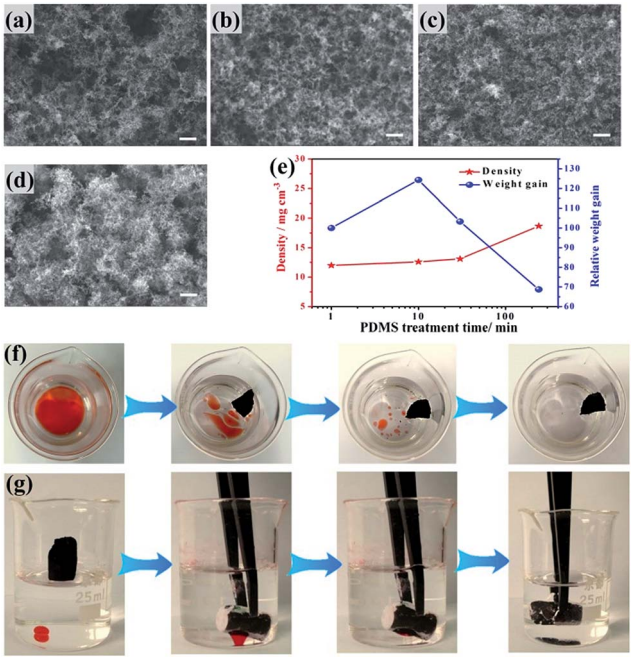

Fig. 4 The SEM images of MWNT aerogels co-heated with PDMS for (a) 0 min, (b) 15 min, (c) 30 min, and (d) 240 min. The scale bar of the SEM images is 1 μm. (e) The MWNT aerogel density and adsorption capacity towards bromobenzene evolution with increasing PDMS treatment time. (f) On-water and (g) underwater adsorption of organic solvent (dyed by Sudan III) by PDMS-treated MWNT aerogels.

heating time, where the weight loading percentage from ~5 to ~50 wt% could be obtained with a treatment time from 10 to 240 minutes (Fig. 4a–e). Although the increased PDMS loading inevitably induced an increased density of the aerogel, the modification of the surface wettability of the gel, from hydrophilic to hydrophobic, may enhance the adsorption performance in a certain range. The oil uptake performance was evaluated using bromobenzene adsorption as an example. The adsorption capacity received a maximum value at a treatment time of ~10 minutes (Fig. 4e), which was approximately 30% higher than that of the unmodified sample. This could be attributed to the net effect of the increased hydrophobicity (the enhanced interactions between the organic solvents and the aerogel) and the increased aerogel density (reduction of the interspace for solvent accommodation). After acquiring high hydrophobicity, the aerogel could be directly applied to an oil/water mixture. As shown in Fig. 4f and g, the aerogels could rapidly remove the organic solvent above or below the water phase within several seconds. From Fig. 4g, the aerogel exhibited a silver colour in water due to the interface formed by entrapped air in the aerogel and the surrounding water outside the aerogel.[15] This phenomenon further proved the high hydrophobicity of the modified aerogel.

Floating-type densitometers

Enjoying a variety of attractive features, *e.g.*, low density, hierarchical pores, and high chemical inertness, carbon-based aerogels should be applied more widely. As a proof-of-concept, we demonstrated an aerogel-based floating-type densitometer. Commercial glass-made floating-type densitometers were commonly manufactured in a floater-like shape with an accurate geometry and a large axial size (typically several tens of centimetres) (Fig. S13†). Although it can give a high accuracy (*ca.* 0.001 g mL^{-1}), the measurable density range was quite narrow (0.1 g mL^{-1}), and the required quantity of test solution was very large (at least several tens of millilitres).

From Fig. 3b and c, aerogels showed similar volume accommodation towards nearly all types of liquid, satisfying their use for densitometers. As shown in Fig. 5a, in this design, the as-prepared aerogel could be visualized as a massless container due to its ultra-low density compared to that of the solvents. For a test solution with a density of ρ_s, the dried aerogel (density of ρ_{gel}) was first saturated with the test solution to acquire an apparent density of $\rho_{apparent} = \rho_s + \rho_{gel} \approx \rho_s$ ($\rho_{gel} \ll \rho_s$). In this way, the density of the test solution was transferred to the aerogel. Then, by placing the aerogel in a series of standard liquids with different densities, ρ_s can finally be constrained in a narrow range by monitoring the position of the aerogel in different standard liquids (excluding the effect time of instantaneous solvent exchange). In practice, ρ_s can be acquired by dropping a series aerogel pieces saturated with different standard solvents in the test solution and then monitor the floating state of each piece.

The feasibility of this method was verified in Fig. 5b–e, where the aerogel floated in a high-density liquid; however, the aerogel sank in a low-density liquid (the high and low densities are referred to ρ_s). The measurement accuracy mainly depends on the aerogel density, where the absolutely true density was obtained when the aerogel density was zero. Otherwise, the acquired density was equal to $\rho_s + \rho_{gel}$. In this case, an accuracy of 0.006 g mL^{-1} could be achieved. Additionally, the high stability of the aerogel in various solutions also facilitates its use for a wide range of test solutions (Fig. S14†).

Compared with commercial glass-made densitometers, the "aerogel densitometer" exhibits several advantages (Table S3†) including less required testing solution, unconstrained device shape, smaller device size, wide measurement range, and so on, which help to facilitate the micro-analysis of various liquids at low cost. According to the measurement principle, the accuracy of the aerogel densitometers could be further improved by reducing the aerogel density, eventually reaching that of commercial densitometers. Therefore, aerogel-based densitometers are good candidates to replace traditional densitometers in the future.

Conclusions

In summary, effective strategies for manipulating the densities of carbon-based aerogels (from 2.5 to 1327 mg cm^{-3}) across a wide range have been proposed by means of altering the type of carbon precursors, the concentration of carbon precursors, the pyrrole concentration and post-treatment conditions. An interesting "Janus face" effect of pyrrole was also revealed in the gelation process. Generally, pyrrole serves as the "spacer" at relatively low concentrations (<*ca.* 5 vol%), while it shows "linker" behaviour at higher concentrations (>*ca.* 5 vol%). Furthermore, using a systematic study, the relationship between the oil adsorption capacity of the aerogel and the aerogel physical parameters (density, porosity and surface wettability) has been established to provide a guideline for designing high-performance sorbents. Following this guideline, a PDMS-modified GNR aerogel with a density of 2.5 mg cm^{-3} was prepared and showed an excellent adsorption capacity towards oils/organics up to 302 times of its own weight. The results were much higher than those of most carbonaceous sorbents previously reported.[10,15,16,20,21,42–44] Moreover, the aerogel can also be directly applied in an oil/water system for water purification after surface modification with a hydrophobic polymer. Finally, a proof-of-concept aerogel-based floating-type densitometer has been proposed to compete with traditional glass-made densitometers. The present work not only provides design principles for carbon-based aerogels for superior oil-uptake performance, but it also opens new windows for expanding the applications of aerogels.

Acknowledgements

The authors thank the financial support of the National Basic Research Program of China (2013CB733700, 2011CB932601), the National Natural Science Foundation of China (21125104, 51373039, 21233001, and 21129001), and the Specialized Research Fund for the Doctoral Program of Higher Education

(20120071130008), and the Program for Innovative Research Team in University (IRT1117).

Notes and references

1 M. A. Shannon, P. W. Bohn, M. Elimelech, J. G. Georgiadis, B. J. Marinas and A. M. Mayes, *Nature*, 2008, **452**, 301.
2 B. Chen, Q. Ma, C. Tan, T. T. Lim, L. Huang and H. Zhang, *Small*, 2015, **11**, 3319.
3 M. Lillo-Ródenas, D. Cazorla-Amorós and A. Linares-Solano, *Carbon*, 2005, **43**, 1758.
4 A. Sayari, S. Hamoudi and Y. Yang, *Chem. Mater.*, 2005, **17**, 212.
5 M. Toyoda, J. Aizawa and M. Inagaki, *Desalination*, 1998, **115**, 199.
6 M. M. Radetic, D. M. Jocic, P. M. Jovancic, Z. L. Petrovic and H. F. Thomas, *Environ. Sci. Technol.*, 2003, **37**, 1008.
7 V. Janout, S. B. Myers, R. A. Register and S. L. Regen, *J. Am. Chem. Soc.*, 2007, **129**, 5756.
8 Y. Xu, S. Jin, H. Xu, A. Nagai and D. Jiang, *Chem. Soc. Rev.*, 2013, **42**, 8012.
9 A. Li, H. X. Sun, D. Z. Tan, W. J. Fan, S.-H. Wen, X. J. Qing, G. X. Li, S. Y. Li and W. Q. Deng, *Energy Environ. Sci.*, 2011, **4**, 2062.
10 R. Du, N. Zhang, H. Xu, N. Mao, W. Duan, J. Wang, Q. Zhao, Z. Liu and J. Zhang, *Adv. Mater.*, 2014, **26**, 8053.
11 R. Du, Z. Zheng, N. Mao, N. Zhang, W. Hu and J. Zhang, *Adv. Sci.*, 2015, **2**, 1400006.
12 P. Si, J. Wang, C. Zhao, H. Xu, K. Yang and W. Wang, *Polym. Adv. Technol.*, 2015, DOI: 10.1002/pat.3538.
13 R. Du, J. Wu, L. Chen, H. Huang, X. Zhang and J. Zhang, *Small*, 2014, **10**, 1387.
14 H. Bi, X. Xie, K. Yin, Y. Zhou, S. Wan, L. He, F. Xu, F. Banhart, L. Sun and R. S. Ruoff, *Adv. Funct. Mater.*, 2012, **22**, 4421.
15 H. Bi, Z. Yin, X. Cao, X. Xie, C. Tan, X. Huang, B. Chen, F. Chen, Q. Yang, X. Bu, X. Lu, L. Sun and H. Zhang, *Adv. Mater.*, 2013, **25**, 5916.
16 X. Gui, J. Wei, K. Wang, A. Cao, H. Zhu, Y. Jia, Q. Shu and D. Wu, *Adv. Mater.*, 2010, **22**, 617.
17 H. Y. Sun, Z. Xu and C. Gao, *Adv. Mater.*, 2013, **25**, 2554.
18 Y. Zhao, C. Hu, Y. Hu, H. Cheng, G. Shi and L. Qu, *Angew. Chem., Int. Ed.*, 2012, **124**, 11533.
19 Y. Wu, N. Yi, L. Huang, T. Zhang, S. Fang, H. Chang, N. Li, J. Oh, J. A. Lee, M. Kozlov, A. C. Chipara, H. Terrones, P. Xiao, G. Long, Y. Huang, F. Zhang, L. Zhang, X. Lepró, C. Haines, M. D. Lima, N. P. Lopez, L. P. Rajukumar, A. L. Elias, S. Feng, S. J. Kim, N. T. Narayanan, P. M. Ajayan, M. Terrones, A. Aliev, P. Chu, Z. Zhang, R. H. Baughman and Y. Chen, *Nat. Commun.*, 2015, **6**, 6141.
20 Z. Y. Wu, C. Li, H. W. Liang, J. F. Chen and S. H. Yu, *Angew. Chem., Int. Ed.*, 2013, **52**, 2925.
21 Z. Y. Wu, C. Li, H. W. Liang, Y. N. Zhang, X. Wang, J. F. Chen and S. H. Yu, *Sci. Rep.*, 2014, **4**, 4079.
22 J. Li, J. Li, H. Meng, S. Xie, B. Zhang, L. Li, H. Ma, J. Zhang and M. Yu, *J. Mater. Chem. A*, 2014, **2**, 2934.
23 S. Barg, F. M. Perez, N. Ni, P. do Vale Pereira, R. C. Maher, E. Garcia-Tuñon, S. Eslava, S. Agnoli, C. Mattevi and E. Saiz, *Nat. Commun.*, 2014, **5**, 4328.
24 J. Zou and F. Kim, *Nat. Commun.*, 2014, **5**, 5254.
25 Z. Chen, W. Ren, L. Gao, B. Liu, S. Pei and H. M. Cheng, *Nat. Mater.*, 2011, **10**, 424.
26 L. Chen, R. Du, J. Zhu, Y. Mao, C. Xue, N. Zhang, Y. Hou, J. Zhang and T. Yi, *Small*, 2015, **11**, 1423.
27 L. Chen, C. Xu, R. Du, Y. Mao, C. Xue, L. Chen, L. Qu, J. Zhang and T. Yi, *J. Mater. Chem. A*, 2015, **3**, 5617.
28 R. Du, N. Zhang, J. H. Zhu, Y. Wang, C. Y. Xu, Y. Hu, N. N. Mao, H. Xu, W. J. Duan, L. Zhuang, L. T. Qu, Y. L. Hou and J. Zhang, *Small*, 2015, DOI: 10.1002/smll.201500587.
29 R. Du, Q. Zhao, N. Zhang and J. Zhang, *Small*, 2015, **11**, 3263.
30 Y. Xu, K. Sheng, C. Li and G. Shi, *ACS Nano*, 2010, **4**, 4324.
31 D. P. Hashim, N. T. Narayanan, J. M. Romo-Herrera, D. A. Cullen, M. G. Hahm, P. Lezzi, J. R. Suttle, D. Kelkhoff, E. Munoz-Sandoval and S. Ganguli, *Sci. Rep.*, 2012, **2**, 363.
32 M. A. Worsley, S. Charnvanichborikarn, E. Montalvo, S. J. Shin, E. D. Tylski, J. P. Lewicki, A. J. Nelson, J. H. Satcher, J. Biener, T. F. Baumann and S. O. Kucheyev, *Adv. Funct. Mater.*, 2014, **24**, 4259.
33 S. M. Jung, H. Y. Jung, M. S. Dresselhaus, Y. J. Jung and J. Kong, *Sci. Rep.*, 2012, **2**, 849.
34 W. He, G. Li, S. Zhang, Y. Wei, J. Wang, Q. Li and X. Zhang, *ACS Nano*, 2015, **9**, 4244.
35 S. Pei and H. M. Cheng, *Carbon*, 2012, **50**, 3210.
36 Y. Tao, X. Xie, W. Lv, D. M. Tang, D. Kong, Z. Huang, H. Nishihara, T. Lshii, B. Li, D. Golberg, F. Kang, T. Kyotani and Q. H. Yang, *Sci. Rep.*, 2013, **3**, 2975.
37 A. Lekawa-Raus, J. Patmore, L. Kurzepa, J. Bulmer and K. Koziol, *Adv. Funct. Mater.*, 2014, **24**, 3661.
38 Y. Li, G. Duan, G. Liu and W. Cai, *Chem. Soc. Rev.*, 2013, **42**, 3614.
39 Y. Li, N. Koshizaki, H. Wang and Y. Shimizu, *ACS Nano*, 2011, **5**, 9403.
40 J. Yuan, X. Liu, O. Akbulut, J. Hu, S. L. Suib, J. Kong and F. Stellacci, *Nat. Nanotech.*, 2008, **3**, 332.
41 H. W. Liang, Q. F. Guan, L. F. Chen, Z. Zhu, W. J. Zhang and S. H. Yu, *Angew. Chem., Int. Ed.*, 2012, **51**, 5101.
42 C. Ruan, K. Ai, X. Li and L. Lu, *Angew. Chem., Int. Ed.*, 2014, **53**, 5556.
43 Z. Niu, J. Chen, H. H. Hng, J. Ma and X. Chen, *Adv. Mater.*, 2012, **24**, 4144.
44 Q. Zhu, Q. Pan and F. Liu, *J. Phys. Chem. C*, 2011, **115**, 17464.